Available online at www.sciencedirect.com
SCIENCE DIRECT®
International Journal of Thermal Sciences 43 (2004) 967–977
International Journal of Thermal Sciences
www.elsevier.com/locate/ijts

Measurement of in-plane diffusivity in non-homogeneous slabs by applying flash thermography

Jean-Claude Krapez [a,*], Leonardo Spagnolo [b], Martin Frieß [c], Hans-Peter Maier [d], Günter Neuer [e]

[a] *ONERA, French Aerospace Research Agency, BP 72, 92320 Châtillon, France*
[b] *Dipartimento di Ingegneria Meccanica e Gestionale, Politecnico di Bari, viale Japigia 182, 70126 Bari, Italy*
[c] *DLR, German Aerospace Center, Institute of Structures and Design, Pfaffenwaldring 38-40, 70569 Stuttgart, Germany*
[d] *Staatliche Materialprüfungsanstalt (MPA), Universität Stuttgart, Germany*
[e] *IKE, Universität Stuttgart, Germany*

Received 19 September 2003; received in revised form 30 January 2004; accepted 9 February 2004

Available online 25 May 2004

Abstract

Through-thickness thermal diffusivity mapping can be performed for a slab material by the classical flash method where a homogeneous and extended source is used to irradiate one surface of the slab and a thermographic camera is used to monitor the temperature evolution on one of the two faces. For measuring the in-plane thermal diffusivity or the diffusivity in one of the principal directions of the plane, a thermal gradient across the plane of the material has to be settled. When such a thermal pulse is applied on a homogeneous slab, the ratio of the Fourier transform of temperature at two different spatial frequencies is an exponential function of time multiplied by the diffusivity in the considered principal direction, which can be used to evaluate it. We propose to use a grid-like mask in front of the flash lamp so that heat is absorbed over a series of periodic parallel strips and the signal-to-noise ratio is increased thereby.

When the material presents an in-plane gradient of in-plane and through-thickness conductivity, we propose to perform the Fourier analysis over a sliding window corresponding to one period of the grid pattern. By this way the profiles of both diffusivities are simultaneously obtained. This approximate method was validated with theoretical temperature profiles obtained by finite difference simulation. The method was applied for in-situ measurement of the diffusivity decrease in tensile samples of C/C-SiC composite material due to the stress-induced density increase of transverse microcracks.

Résumé

La technique flash classique permet de mesurer la diffusivité d'un matériau orthotrope dans la direction normale à sa surface. Une mesure thermographique avec chauffage étendu, suivie d'une identification locale, pixel par pixel, permet d'en établir une cartographie approchée. Une façon d'accéder à la diffusivité dans le plan de la pièce (ou dans les directions principales du plan d'une plaque orthotrope) consiste à appliquer un chauffage non uniforme sur l'une des deux faces et à analyser l'évolution du champ thermique sur l'une ou l'autre des faces. Dans le cas d'un matériau homogène, l'étude du rapport de la transformée de Fourier de la température suivant une direction principale du plan, à deux fréquences spatiales différentes, est une fonction exponentielle du temps multiplié par la diffusivité dans la direction considérée, ce qui en permet l'identification. Le fait de déposer la chaleur sur un ensemble de bandes régulièrement espacées, principe de la méthode flash avec masque périodique, fournit un rapport signal sur bruit élevé. L'étude des transformées de Fourier d'ordre 0 et 1 conduit simultanément aux diffusivités dans le plan et dans la direction normale.

Dans le cas où les conductivités correspondantes dépendent de l'abscisse, l'approche locale que nous proposons consiste à appliquer les transformées de Fourier sur une fenêtre glissante de largeur limitée à une période de la grille. Cette méthode approchée a été validée sur des profils théoriques de température obtenus pas différences finies. Elle a été utilisée pour quantifier la réduction de la diffusivité transverse dans des éprouvettes de traction en matériau composite C/C-SiC, réduction due à l'augmentation de la densité des microfissures à mesure que la contrainte augmente.

Keywords: Thermography; Thermal diffusivity; Anisotropy; In-plane diffusivity; Diffusivity profile; Ceramic matrix composites; Transverse cracks

* Corresponding author.
E-mail address: krapez@onera.fr (J.-C. Krapez).

1290-0729/$ – see front matter
doi:10.1016/j.ijthermalsci.2004.02.003

Mots-clés : Thermographie ; Diffusivité thermique ; Anisotropie ; Diffusivité dans le plan ; Profil de diffusivité ; Composites à matrice céramique ; Fissures transverses

1. Introduction

Many composite materials are used for their thermal characteristics, as in the case of carbon brakes and thermal protections for hypersonic vehicles. In the first example the material must simultaneously diffuse heat away from the thermally stressed areas and offer a high thermal capacity. On the opposite, the material in the second example must present a low thermal conductivity. The non-destructive measurement of diffusivity is thus of prime importance for the quality control of such products. Furthermore, as the composite materials are often anisotropic from the thermal point of view, one may have to measure the three principal thermal diffusivities.

The through-thickness thermal diffusivity can be measured by the classical flash method (either in one-side or in two-side configuration). A pulsed source of radiation, i.e., a laser or a flash lamp, is used to heat one side of the sample, while the temperature response of either front or rear surface is measured by a thermocouple or, without any contact, by an infrared detector. If an extended source is used to provide a uniform heat input and a thermographic camera is used to follow the temperature distribution evolution, a map of the through-thickness thermal diffusivity can be obtained for the tested slab in a single experiment [1–5].

In order to measure the in-plane diffusivity of a plate-like orthotropic sample and, in particular, the diffusivity in one of the principal directions of the plane, a thermal gradient across the plane of the material has to be settled. For this purpose, different experimental configurations and data processing procedures have been proposed in the past [6–26]. Heat can be applied over a point [7–12], a Gaussian distribution (spot or strip) [13,14], a disk area [15,16], an annular area [16,17], a line or a strip [18–21], a half plane [22], or a square corner [23]. Recently it was also suggested to use a moving line heat source [24] or a heat pulse with random distribution [25].

Present paper deals with the grid-like mask technique that we recently proposed for the characterisation of homogeneous materials [26,27]. With this technique a grid-like mask is put between the radiative heat source and the sample while an IR camera is monitoring the temperature on the rear side of the sample. It is then possible to follow, at the same time, two phenomena: the through-thickness diffusion and the in-plane diffusion of heat from the illuminated strips to the strips that were in the grid shadow. The use of a periodic line pattern was suggested a few years ago in the field of nondestructive testing for the purpose of crack detection: "forced diffusion" was obtained by continuously moving the line pattern in the perpendicular direction [28].

Present paper deals with the static grid-like mask technique. First purpose is to present a theoretical analysis about the identification procedure and about the measurement accuracy in the case of homogeneous materials. The application is then extended to the control of materials that present a transverse gradient regarding both in-plane and through-thickness diffusivities. As a matter of fact, the problem of imaging the in-plane diffusivity has received much less attention than the one of imaging the through-thickness diffusivity [24,25]. The proposed approach consists in applying the previously described identification procedure on a local basis through the use of a sliding window. By this way it is possible to get approximate profiles of both in-plane and through thickness thermal diffusivities.

The grid-flash thermography technique can actually be applied in the one-side or in the two-side configuration. Experiments will be reported for the two-side configuration. They refer to the in-situ characterisation of C/C-SiC dog-bone samples under tensile stress while experiencing cracking. Profiles of both longitudinal and transverse diffusivities will be presented with respect to the applied stress.

2. Description of the basic experiment

A typical set-up for flash thermography with a grid-like mask is represented in Fig. 1. The two-sided configuration (rear face thermography) is here considered but the one-sided configuration is also possible (front-face thermography where the lamp, the grid and the camera are on the same side of the sample). With a grid-like mask represented like in Fig. 1, the purpose is to map the principal diffusivities in x and z directions.

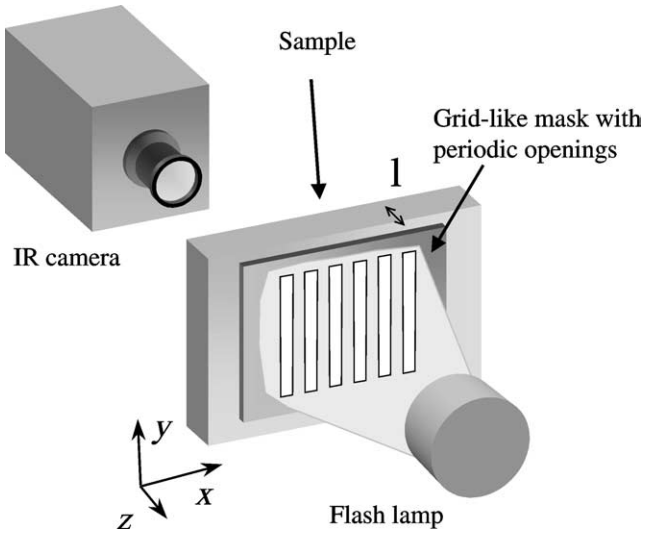

Fig. 1. Flash thermography with a grid-like mask. Example of the two sided configuration.

Nomenclature

a	diffusivity	$m^2 \cdot s^{-1}$
A	thermal aspect ratio (Eq. (14))	
C	specific heat	$J \cdot kg^{-1}$
h_0, h_l	heat losses coefficients (front and rear face)	$W \cdot m^{-2} K^{-1}$
Fo_x, Fo_z	Fourier number with respect to x, z-direction	
k	conductivity	$W \cdot m^{-1} \cdot K^{-1}$
l	slab thickness	m
N_x, N_y	number of pixels in x, y-direction	
p	Laplace variable	s^{-1}
$Q(x, y, z)$	absorbed heat density distribution	$J \cdot m^{-2}$
Q_0	absorbed heat density over the heated strips	$J \cdot m^{-2}$
t	time	s
T	temperature	K

Greek symbols

β_1, β_2	estimated parameters	
Δ	heat distribution period (grid pitch)	m
ρ	density	$kg \cdot m^{-3}$
σ	temperature standard deviation	K
ω	Fourier variable	m^{-1}
$\boldsymbol{\Psi}, \boldsymbol{\Omega}$	covariance matrices (Eq. (18))	

Notations

$\overline{F}$	Laplace transform of F
$L^{-1}\{\overline{F}\}$	inverse Laplace transform of $\overline{F}$
$\widetilde{F}$	Fourier transform of F (in x- or y-direction)

Underscript

0, 1	Fourier transform of order 0 and 1 (at $\omega_x = 0$ and at $\omega_x = \Delta^{-1}$)

3. Theoretical analysis

3.1. Thermal model

The model that was considered for the heat transfer calculations and for the parameter identification is described in Fig. 2. Its main features can be listed as following:

– infinite orthotropic plate with thermal properties: ρC, a_x, a_y, $a_z(z)$, uniform thickness, and uniform initial temperature distribution;

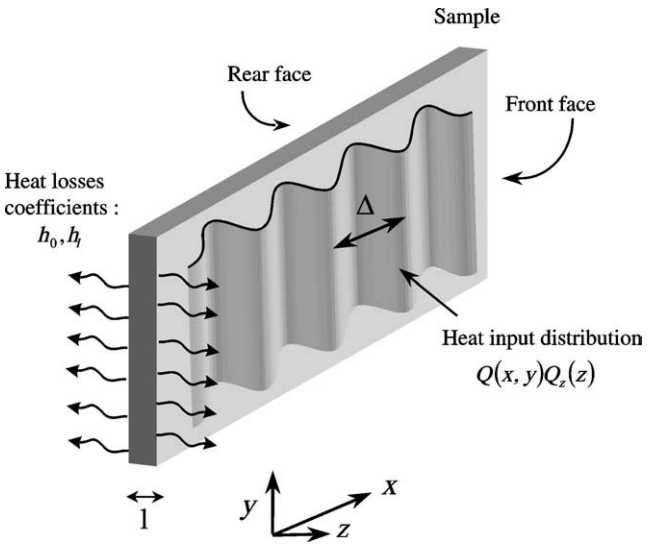

Fig. 2. Considered model: an orthotropic plate (principal diffusivities: a_x, a_y, a_z) submitted to linear heat losses (coefficients h_0, h_l, respectively on rear and front face), receives a short heat pulse with distribution $Q(x, y)Q_z(z)$. This figure illustrates the particular case of a periodic distribution in x-direction (period Δ).

– linear heat losses on both faces with uniform and constant coefficients h_0, h_l;
– Dirac pulse with non-uniform distribution $Q(x, y)Q_z(z)$ (a periodic pattern in one direction—period Δ—like the one represented in Fig. 2, is particularly suitable, as will be seen later, but the initial theoretical development is valid for any in-plane distribution $Q(x, y)$);

The heat equation, the initial and boundary conditions for the present problem are:

$$\rho C \frac{\partial T}{\partial t} = k_x \frac{\partial^2 T}{\partial x^2} + k_y \frac{\partial^2 T}{\partial y^2} + \frac{\partial}{\partial z}\left[k_z(z) \frac{\partial T}{\partial z}\right] \tag{1}$$

$$T(x, y, z, 0) = Q(x, y)Q_z(z)/\rho C \tag{2}$$

$$-k_z \frac{\partial T}{\partial z}\Big|_{z=0} = -h_0 T(x, y, 0, t) \tag{3}$$

$$-k_z \frac{\partial T}{\partial z}\Big|_{z=l} = h_l T(x, y, l, t) \tag{4}$$

3.2. Identification relationship

We make use of the Fourier–Laplace transform defined by:

$$\overline{\overline{\widetilde{T}}}(\omega_x, \omega_y, z, p) = \int_{t'=0}^{t'=\infty} \int_{x'=-\infty}^{x'=\infty} \int_{y'=-\infty}^{y'=\infty} T(x', y', z, t) \times e^{i\omega_x x'} e^{i\omega_y y'} e^{-pt'} \, dt' \, dy' \, dx' \tag{5}$$

it leads to the equation:

$$\left(\rho C p + k_x \omega_x^2 + k_y \omega_y^2\right) \overline{\overline{\widetilde{T}}} - \overline{\overline{\widetilde{Q}}} Q_z(z) = \frac{\partial}{\partial z}\left[k_z(z) \frac{\partial \overline{\overline{\widetilde{T}}}}{\partial z}\right] \tag{6}$$

Let $T_z(z, t)$ be the solution of the heat diffusion problem when the plate is heated uniformly in x- and y-directions

with intensity $Q_z(z)$, i.e., 1D diffusion in a slab of conductivity $k_z(z)$. Thanks to the Laplace shift property, one thus has the following relation:

$$\begin{aligned}&\tilde{\tilde{\tilde{T}}}(\omega_x,\omega_y,z,t)\\&\quad=\tilde{\tilde{\tilde{Q}}}(\omega_x,\omega_y)T_z(z,t)\exp\bigl(-a_x\omega_x^2t-a_y\omega_y^2t\bigr)\end{aligned}\tag{7}$$

where a_x and a_y are the thermal diffusivities along the x-axis and the y-axis. It follows that, at any depth, the double spatial Fourier transform $\tilde{\tilde{\tilde{T}}}$ of the temperature at $(\omega_x,\omega_y)=(0,0)$, i.e., the spatial integral along x, and y-directions, has the same evolution as the temperature induced by a uniform heating with a heat input equal to $\tilde{\tilde{\tilde{Q}}}(0,0)Q_z(z)$ (this result is also valid for a limited plate provided the edges are isolated). For this reason, assuming now that the diffusivity $a_z(z)$ is constant, and that $Q_z(z)=\mathrm{Dirac}_{z=l}(z)$, one can then evaluate the through-thickness thermal diffusivity a_z by applying on $\tilde{\tilde{\tilde{T}}}(0,0,t)$ the classical algorithms devoted to the well-known rear-face flash experiments, as, for example, the moment method [29].

In Eq. (7), one can eliminate T_z to get the following relation:

$$\begin{aligned}&\tilde{\tilde{\tilde{T}}}(\omega_x,\omega_y,z,t)/\tilde{\tilde{\tilde{T}}}(0,0,z,t)\\&\quad=\tilde{\tilde{\tilde{Q}}}(\omega_x,\omega_y)/\tilde{\tilde{\tilde{Q}}}(0,0)\exp\bigl(-a_x\omega_x^2t-a_y\omega_y^2t\bigr)\end{aligned}\tag{8}$$

This relation is valid at any depth, in particular on the front and rear faces. It is important to notice that Eq. (8) is valid even in the presence of losses on any of the two faces of the sample. Furthermore, it is not required that heat is absorbed on the surface, i.e., it is valid for any in-depth distribution of energy $Q_z(z)$. Therefore the method can be applied on non-opaque materials, provided that the heat distribution can be separable according to: $Q(x,y)Q_z(z)$.

In practice, we use a periodic distribution in the x-direction with period Δ. The temperature is integrated along y direction between $-Y$ and $+Y$, and we use a Fourier transform in x-direction defined on an integer number of periods $n\Delta$ (the axis origin is chosen so that the heat flux periodic profile is even and maximum at $x=0$):

$$\begin{aligned}\tilde{\tilde{\tilde{T}}}(\omega_x,0,z,t)=\frac{1}{n\Delta}\frac{1}{2Y}\int_{x'=0}^{x'=n\Delta}\int_{y'=-Y}^{y'=+Y}\\\times T\bigl(x',y',z,t\bigr)\cos\bigl(\omega_x x'\bigr)\,\mathrm{d}y'\,\mathrm{d}x'\end{aligned}\tag{9}$$

The following linear relationship can thus be used in order to infer the thermal diffusivity in *x-direction*:

$$\begin{aligned}&\mathrm{Ln}\bigl[\tilde{\tilde{\tilde{T}}}(\omega_x,0,z,t)/\tilde{\tilde{\tilde{T}}}(0,0,z,t)\bigr]\\&\quad=\mathrm{Ln}\bigl[\tilde{\tilde{\tilde{Q}}}(\omega_x,0)/\tilde{\tilde{\tilde{Q}}}(0,0)\bigr]-a_x\omega_x^2t\end{aligned}\tag{10}$$

This relation is in particular valid on the rear face at $z=0$. Furthermore, due to the heat distribution periodicity, we are mostly interested in the Fourier transform at the angular frequency $\omega_x=2\pi/\Delta$. By performing a linear regression on the time plot of $\mathrm{Ln}[\tilde{\tilde{\tilde{T}}}(\omega_x,0,0,t)/\tilde{\tilde{\tilde{T}}}(0,0,0,t)]$ one can immediately get through its slope an evaluation of a_x. The diffusivity in the y-direction is obtained by rotating the mask by 90° and then repeating the experiment.

3.3. Homogeneous materials: Influence of the measurement noise

As pinpointed in [19], the great number of data points provided by infrared thermography may result in a substantial noise reduction of statistical origin. In order to highlight the effect of the temperature signal noise on the error of the inferred in-plane diffusivity, one will consider the simple case of an adiabatic plate that is heated on its front surface over a series of parallel strips.

Let us assume that heat is absorbed on the surface $z=l$ and that its distribution is periodic with square shape in x direction whereas uniform in y direction. Over the heated strips, the heat density is Q_0. If one assumes that there are no heat losses, one has:

$$T_0(t)\equiv\tilde{\tilde{\tilde{T}}}(0,0,0,t)=\frac{Q_0}{2\rho Cl}f(t)\tag{11}$$

$$T_1(t)\equiv\tilde{\tilde{\tilde{T}}}(\omega_x,0,0,t)=\frac{2}{\pi}T_0(t)\exp\bigl(-a_x\omega^2t\bigr)\tag{12}$$

where the normalised temperature $f(t)$ is expressed by:

$$f(t)=\frac{l^2}{a_z}L^{-1}\left\{\frac{1}{q\,\mathrm{sh}\,q}\right\},\quad q=\sqrt{p/a_z}\tag{13}$$

where p is the Laplace variable.

The *thermal aspect ratio* of the considered periodic pattern, with respect to the sample thickness l and its anisotropy factor, is defined by:

$$A\equiv\Delta/l\sqrt{a_z/a_x}\tag{14}$$

It is merely the square root of the diffusion times along Δ and along l in the two principal directions.

Previous works [26,27] showed that the accuracy of the measurements increases with the thermal aspect ratio, however the improvement is negligible for thermal aspect ratio values greater than 4 or 5 (of course, in order to properly choose the grid pitch, one has to make a first assumption regarding the ratio of the principal diffusivities, the grid size can be adjusted in a second step). In the following we propose a more complete discussion on the diffusivity identification procedure and on the influence of experimental noise on the diffusivity uncertainty.

The time evolution of $T_0(t)$ and $T_1(t)$ is given in Fig. 3 for a series of values of the *thermal aspect ratio* between 1.2 and 10. $T_0(t)$ rises to the adiabatic level whereas $T_1(t)$ first rises and then vanishes back to 0. A higher value of the thermal aspect ratio leads to a maximum of higher level and later occurrence.

The measured temperature at a given pixel is an estimator of the temperature. The errors are assumed to have

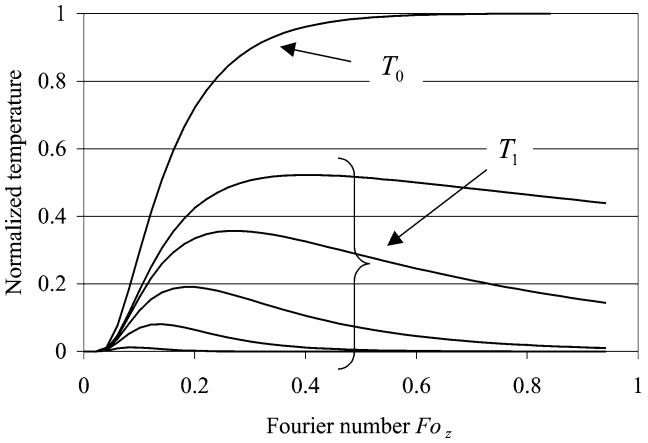

Fig. 3. Evolution of the mean temperature $T_0(t)$ and of the Fourier transform $T_1(t)$ on the rear side of the sample. Both functions are normalised by the adiabatic level. The reduced time that was chosen here is the Fourier number $Fo_z \equiv a_z t/l^2$. For $T_1(t)$ the thermal aspect ratio A is, from top to bottom: 10, 5, 3, 2 and 1.2.

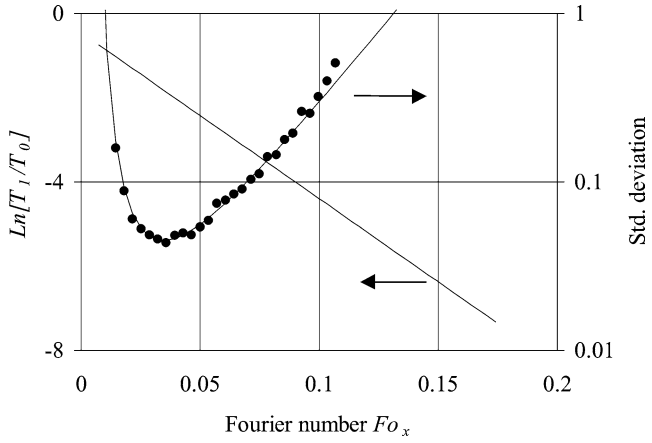

Fig. 4. Evolution of the observable variable $\mathrm{Ln}[T_1(t)/T_0(t)]$ for a thermal aspect ratio A equal to 2. The observable standard deviation is plotted on the right axis for the case of a noise standard deviation $\sigma/T_{0\max}\sqrt{N_x N_y}$ of 0.005. The continuous line was obtained through linear approximation (Eq. (16)); the dots were obtained through a statistical analysis. The reduced time that was chosen here is the Fourier number $Fo_x \equiv a_x t/\Delta^2 = Fo_z/A^2$.

zero mean, constant standard deviation σ, and to be independent. In that case, the covariance matrix of the errors on $[T_0(t) \quad T_1(t)]^t$ is given by [19]:

$$\mathrm{cov}\big(\big[T_0(t) \quad T_1(t)\big]^t\big) = \frac{\sigma^2}{N_x N_y}\begin{bmatrix} 1 & 0 \\ 0 & 1/2 \end{bmatrix} \tag{15}$$

The averaging along y direction between $-Y$ and $+Y$ is performed over N_y pixels, whereas the Fourier transform along x direction is performed over N_x pixels which correspond to an integer number of spatial periods $n\Delta$. Eq. (15) assumed negligible quadrature errors.

The standard deviation of the observable $\mathrm{Ln}[T_1(t)/T_0(t)]$ can be obtained through a linear approximation by assuming that the errors on $T_1(t)$, respectively $T_0(t)$, are small with respect to $T_1(t)$, respectively $T_0(t)$. In that case, one has:

$$Std\big\{\mathrm{Ln}\big[T_1(t)/T_0(t)\big]\big\} \approx \frac{\sigma}{\sqrt{N_x N_y}}\sqrt{\frac{1}{2T_1(t)^2} + \frac{1}{T_0(t)^2}} \tag{16}$$

We also estimated $Std\{\mathrm{Ln}[T_1(t)/T_0(t)]\}$ through a Monte Carlo analysis by adding to the thermograms in Fig. 3 a Gaussian noise. In Fig. 4 the results are plotted for the particular case of a thermal aspect ratio of 2 and a noise standard deviation of 0.005. The approximate relation in Eq. (16) provides satisfactory results except at short and long times where a small deviation can be observed. This occurs when $T_0(t)$ or $T_1(t)$ reach values that are lower than about twice the noise standard deviation. Otherwise the use of Eq. (16) is justified.

The in-plane diffusivity a_x is obtained through maximum likelihood estimation. It is based on the linear relationship in Eq. (10). All data between time t_1 and t_m on the thermograms are used for the estimation. The sensitivity matrix with respect to the vector of parameters

$[\beta_1 \quad \beta_2]^t \equiv \big[-a_x\omega_x^2 \quad \mathrm{Ln}\big[\tilde{\tilde{Q}}(\omega_x,0)/\tilde{\tilde{Q}}(0,0)\big]\big]^t$ is:

$$\mathbf{X} = \begin{bmatrix} t_1 & 1 \\ \dots & \dots \\ t_m & 1 \end{bmatrix} \tag{17}$$

The covariance matrix of the observable variable is a diagonal matrix $\boldsymbol{\Psi} = \frac{\sigma^2}{T_{0\max}^2 N_x N_y}\boldsymbol{\Omega}$ where the elements Ω_{ii} are given by:

$$\Omega_{ii} = \frac{T_{0\max}^2}{2T_1(t_i)^2} + \frac{T_{0\max}^2}{T_0(t_i)^2} \tag{18}$$

The covariance matrix of $[\beta_1 \quad \beta_2]^t$ is obtained through [30]:

$$\mathrm{cov}\big([\beta_1 \quad \beta_2]^t\big) = \frac{\sigma^2}{T_{0\max}^2 N_x N_y}\big(\mathbf{X}^t\boldsymbol{\Omega}^{-1}\mathbf{X}\big)^{-1} \tag{19}$$

The standard deviation of the inferred diffusivity is plotted in Fig. 5 depending on the choice for the time interval $[Fo_{x1}, Fo_{xm}]$ that is used for the identification. In the first case (curve a) Fo_{x1} was fixed at 0 and the right limit Fo_{xm} was progressively increased from 0, whereas in the second case (curve b) Fo_{xm} was fixed at a large value, i.e., 0.17, and the left limit Fo_{x1} was progressively decreased. One can notice that the standard deviation reaches a bottom level when Fo_{xm} is increased, respectively when Fo_{x1} is decreased. The bottom level is reached by 5% when Fo_{xm} is increased to about 0.1, respectively when Fo_{x1} is decreased to about 0.02. For the parameter identification process it is thus useless to take into account the leftmost part and the rightmost part of the thermograms. For the particular case of a thermal aspect ratio of 2, the "useful" part of the thermograms is $Fo_x \in [0.02, 0.1]$. At the left edge, respectively right edge, $T_1(t)$ is only about ten times, respectively two times, higher than the noise level.

The minimum std. dev. of diffusivity can be normalised by the relative temperature noise $\sigma/T_{0\max}\sqrt{N_x N_y}$ and by the square root of the Fourier step $\sqrt{\Delta Fo_x}$ relative to the data

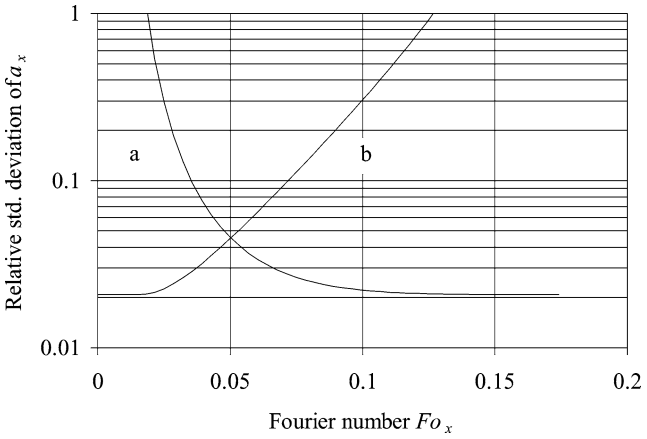

Fig. 5. Relative standard deviation of the inferred in-plane diffusivity depending on the time interval $[Fo_{x1}, Fo_{xm}]$ used for the parameter identification. Curve a: left limit is fixed at 0, curve b: right limit is fixed at 0.17. Thermal aspect ratio $A = 2$, noise of standard deviation $\sigma/T_{0\max}\sqrt{N_x N_y} = 0.005$.

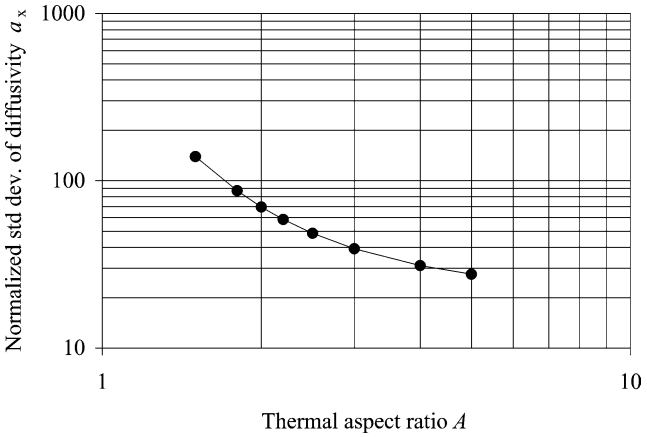

Fig. 6. Normalised standard deviation of in-plane diffusivity a_x vs. the thermal aspect ratio A (see text).

storage rate. The influence of the thermal aspect ratio A on the normalised std. dev. of in-plane diffusivity a_x is plotted in Fig. 6. When the thermal aspect ratio is 2, the normalised std. dev. is 70. It means that if temperature is measured with a standard deviation of $\sigma/T_{0\max}\sqrt{N_x N_y} = 0.01$, and with a time step corresponding to $\Delta Fo_x = 0.0025$, the best achievable relative standard deviation for in-plane diffusivity is $70 \times 0.01 \times \sqrt{0.0025} = 0.035$.

One can notice in Fig. 6 that the results worsen very rapidly when the thermal aspect ratio A decreases. As a matter of fact, it seems preferable to use a mask with a high aspect ratio. However, when A is set to a high value, namely 5 or more, the time intervals that are necessary for the in-plane and the out-of-plane diffusivity identifications become very different. Indeed, for the out-of plane diffusivity identification, it is not necessary to consider the late evolution corresponding to Fo_z larger than about 0.7, i.e., when the maximum of $T_0(t)$ is close to be reached. On the opposite, for the in-plane diffusivity identification, one can consider the thermal evolution until $T_1(t)$ drops to about twice the noise level (this corresponds to $Fo_x \approx 0.1$ in the particular case of a noise level of 0.005). If one chooses to perform a simultaneous identification of both diffusivities, and if one uses a mask with a high aspect ratio in order to identify the in-plane diffusivity with a good precision, it will be required to perform the thermographic acquisition simultaneously over a long period and with a high data acquisition rate. At this point the question could be raised about the requirement of simultaneous identification of a_x and a_z. Indeed, if the tested material is expected to have a uniform in-plane diffusivity and a uniform out-of-plane diffusivity, the characterisation could be performed sequentially: a_z could be measured by applying the classical flash method (without any mask), then a_x could be measured by applying the flash technique with a mask having an aspect ratio typically higher than 5. Some considerations may however prevent from increasing the aspect ratio too much. The lateral size of the tested piece is a first natural limitation. Then, the heat losses (convection, radiation) may provide some drawbacks. As a matter of fact, although the heat losses on the front face and on the rear face do not intervene in the in-plane diffusivity identification relationship (Eq. (10)), they however have an influence on the standard deviation of the observable parameter (Eq. (16)) via their influence on $T_0(t)$ and on $T_1(t)$. At later times, the standard deviation rises more rapidly than it was depicted in Fig. 4 which corresponded to the adiabatic case. A parametric analysis based on the Biot number related to the heat losses would thus be required in order to identify for each Biot number the optimal aspect ratio for the mask.

Finally, one should mention an important case where it is recommended to use a grid with a low aspect ratio: it is aimed to the control of non-homogeneous materials in which the profile of the in-plane diffusivity is to be determined. This particular application of the grid method will be dealt in the following part of the paper.

3.4. Heterogeneous materials: Diffusivity profile identification

The purpose is now to assess the potential of the grid technique for the characterisation of *heterogeneous* materials in which the diffusivities may present some variations in the x direction: $a_x(x)$, $a_z(x)$. One way to extract from the thermographic data obtained by the grid technique local information is to reduce the size of the domain over which the identification is usually performed. Instead of performing the Fourier transform over several spatial periods of the grid, one can restrict it to the smallest possible area, namely one period Δ of the grid-like mask. Data processing can then be performed on a *sliding window* of this width. Temperature is first averaged in y-direction, and then the following operations are performed:

– temperature is averaged in x direction over the Δ-window; this mean temperature $T_0(t) \equiv \widetilde{\widetilde{T}}(0,0,0,t)$ is

used to identify a local value of the through-thickness diffusivity $a_z(x)$;
– through linear parameter identification, the local temperature spatial half-amplitude at frequency Δ^{-1}, i.e., $T_1(t) \equiv |\tilde{\tilde{T}}(\omega_x, 0, 0, t)|$, is calculated at first. Then, through a maximum likelihood estimation based on Eq. (10), a local value of the in-plane diffusivity $a_x(x)$ is evaluated.

These local values of in-plane and out-of-plane diffusivity yield two profiles that are expected to be fairly close to the sliding averages of the two real diffusivity profiles. The actual efficiency of this approximate approach will be assessed by applying it on theoretical data. These data were obtained by numerical simulation of heat diffusion in a material that presents a diffusivity drop in a particular $[x_1, x_2]$ interval. The considered material has an in-plane nominal diffusivity of 11 $\text{mm}^2\cdot\text{s}^{-1}$ and a through-thickness nominal diffusivity of 7.5 $\text{mm}^2\cdot\text{s}^{-1}$ (typical values for C/C-SiC material as will be seen later). The plate is 3 mm thick and it is heated on the front face over parallel strips that are 4 mm wide ($\Delta = 8$ mm). The plate has a defective region 37 mm wide starting at $x_1 = 52$ mm where both diffusivities are 20% lower than the corresponding nominal values.

The heat diffusion problem was solved by finite differences on a 256×30 rectangular mesh corresponding to a 128 mm $\times$ 3 mm section. The evolution of the temperature profile on the rear side is described in Fig. 7. Behind the defective region, the mean value of the temperature modulation rises lately because of a reduced a_z value. The relative amplitude of the modulation reaches its maximum later because of the reduced a_x value. By analysing the temperature profile evolution locally, i.e., in an 8 mm sliding window, one is able to evaluate the local apparent in-plane and through-thickness diffusivities.

The diffusivity values as obtained by applying the procedure described above are reported in Fig. 8. The inverted profiles can be compared with the true square shaped profiles. A second simulation was performed by moving the heat input distribution by a quarter of a period. The reason is as follows. It is clear that in the case of a homogeneous material, the normal planes passing through the middle of the lighted strips and through the middle of the obscured strips see no transverse heat flow. This is due to the symmetry of the heat input distribution. Therefore the sensitivity to the in-plane diffusivity vanishes in the vicinity of these two series of planes. If a perpendicular crack were present along one of these planes, it would be left undetected on the temperature profiles. A remedy to eliminate these "dead zones" in the material simply consists in moving the grid by $\Delta/4$ and in repeating the experiment (another remedy consists in "breaking" the symmetry and using, for example, a random distribution [25]). A second couple of profiles is thus obtained that is similar but not equal to the first one. Apart from the vicinity of the sudden diffusivity drop, the diffusivity values are correctly retrieved (notwithstanding a small bias due to the discretisation error inherent to the finite difference method). Present technique however cannot invert sharp diffusivity variations with a good precision like those of a square profile. Sudden variations are smoothed like through local averaging over a window whose width is between Δ and 2Δ.

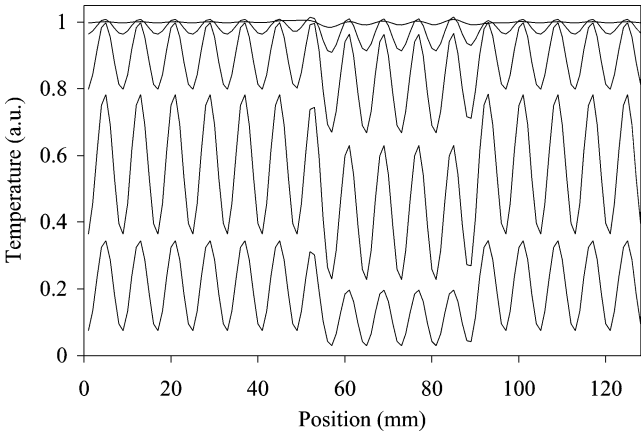

Fig. 7. Computed temperature profile on the rear side of a 3 mm plate in which, between position $x = 52.5$ mm and $x = 89$ mm, both diffusivities a_x and a_z drop by 20% from, respectively, 11 and 7.5 $\text{mm}^2\cdot\text{s}^{-1}$. From bottom to top, time from the heat pulse is: 0.1, 0.18, 0.36, 0.6 and 1 s.

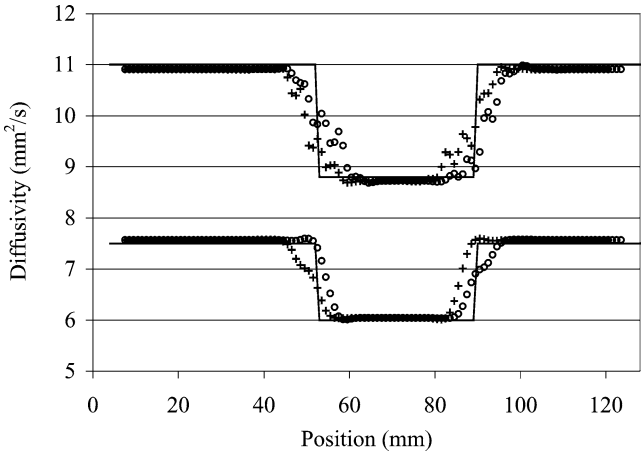

Fig. 8. Identified diffusivity profiles from the theoretical temperature profiles like those reported in Fig. 7. On top is the in-plane diffusivity, at the bottom is the through-thickness diffusivity (nominal values are, respectively, 11 and 7.5 $\text{mm}^2\cdot\text{s}^{-1}$). Profiles in continuous lines are the true ones, the other four profiles are the inversion results (the profiles with crosses where obtained after the heat input distribution was moved by $\Delta/4$).

In Fig. 9 the same work was performed after having added a Gaussian noise to the simulated thermograms before the inversion. The level of noise was 2% of the adiabatic temperature level. The amplitude of the true profile variations is well retrieved despite unavoidable erratic fluctuations. According to Fig. 6, the expected relative error for in-plane diffusivity is 1.7% (sampling is performed at 109 s^{-1}). The calculated standard deviation in the defect-free region of a_x profiles is actually in the range 2.3–2.8%, i.e., not far from the expected value. This single illustration

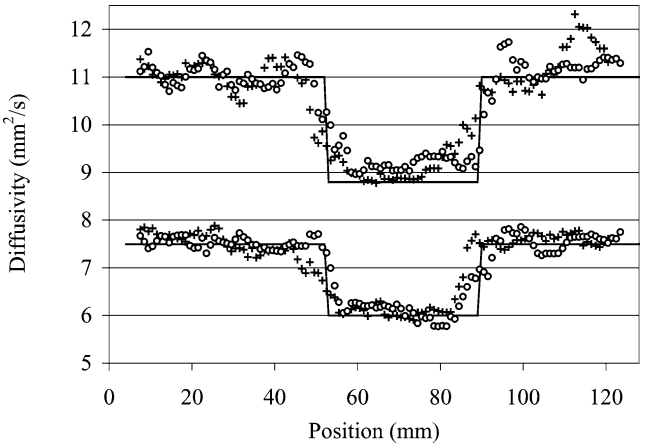

Fig. 9. Same when 2% Gaussian noise is added to the thermograms before applying the inversion.

cannot be considered as a general proof of the efficiency of the proposed inversion method. It however seems that this method is well suited for smooth diffusivity profiles. In the case of rapid variations, the inversion merely provides a filtered image of the true profile. The use of finer grids is thus recommended in order to capture smaller details. There is however some trade-off because fine grids (i.e., low thermal aspect ratio values) yield low signal to noise ratio (see Fig. 6).

4. In-situ characterisation a C/C-SIC composite

The characterised material is a composite material used for space applications, brake discs and pads and for tubes in high and ultrahigh temperature heat exchangers. It is made of carbon fibres in a carbon matrix in which Si at liquid phase was infiltrated and in-situ reacted with carbon to form the SiC matrix [31]. The microstructure (Fig. 10) shows dense C/C segments which are surrounded by the SiC matrix and some residual Si. The important thermal characteristics of this composite, such as its resistance at very high temperatures, make it become one of the most appreciate materials for aerospace applications, above all for thermal barriers.

The purpose of this work was to evaluate the presence of micro-cracks inside the material. Different dilatation coefficients of the matrix and of the fibres cause the appearance of these cracks during the forming process, as shown in Fig. 10. Micrographic analysis demonstrated that the density of micro-cracks (<150 μm) *increases with the applied stress*. In fact the reason of the material failure is supposed to be the excessive number of micro-cracks.

There was a need for a non-destructive characterisation method that would provide an indication on the micro-cracks density. Such a method would avoid the costly and lengthy micrograph analysis. The local measurement of in-plane thermal diffusivity by the grid method could provide an answer to this problem as this thermal parameter is thought

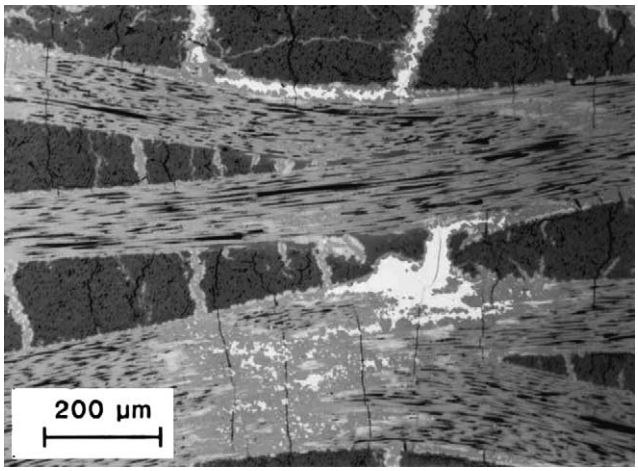

Fig. 10. Micrograph of a polished C/C-SiC sample. Micro-cracks can be seen between the fibres inside a bundle (dark areas), as well as across the fibres (clear areas).

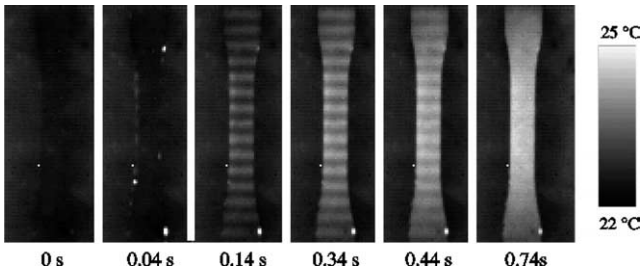

Fig. 11. Successive IR images of the rear face of a particular C/C-SiC tensile sample during a grid-flash experiment.

to be correlated with the distribution of transverse micro-cracks.

The tested C/C-SiC samples have a dog-bone shape. They are 3 mm thick and the central part with constant width is 12 mm wide by 40 mm long. While being stressed in a mechanical test machine, the samples were submitted to successive grid-flash experiments in the transmission configuration. A flash lamp was used to provide pulses 2 to 4 ms long with 0.5 J·cm^{-2} energy density. A grid-like mask, with a 7.35 mm period, was put close to the sample on the flash lamp side. A focal plane array IR camera (Amber AE4128, 128 × 128 detectors, NETD = 7 mK), was used to monitor the temperature of the other face of the sample.

In Fig. 11 is reported a series of IR images relative to a single test. Shortly after the flash pulse, the strips that have been directly lighted by the flash lamp, reach an appreciable temperature level on the rear side letting the periodic pattern becoming more and more visible. In the meantime the lateral diffusion tends to homogenise the temperature of the sample. It takes about 1 s for the sample to pass from the initial room temperature to a nearly uniform 2 °C higher level.

Fig. 12 illustrates the sliding window procedure. The average temperature $T_0(t)$, the hafl-amplitude of the spatial modulation $T_1(t)$ and the observable variable $\mathrm{Ln}[T_1(t)/T_0(t)]$

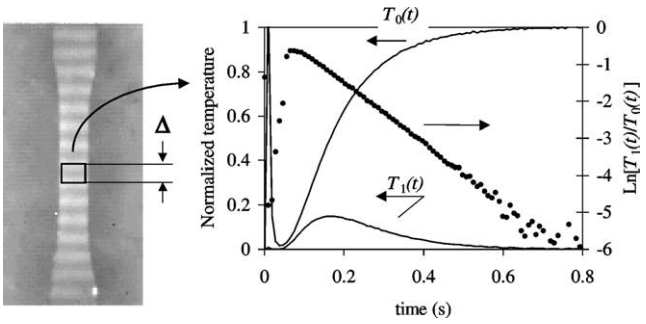

Fig. 12. Parameter identification with a sliding window whose width corresponds to one period of the grid. On the right are plotted, for a particular position of the sliding window, the average temperature, $T_0(t)$, the first Fourier component of temperature $T_1(t)$, and the chosen observable variable $\mathrm{Ln}[T_1(t)/T_0(t)]$.

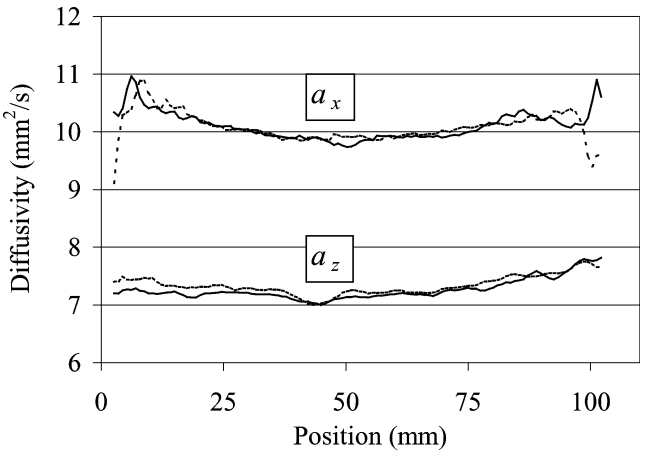

Fig. 13. Diffusivity profiles obtained from the IR sequence in Fig. 11, where the sample was submitted to a 120 MPa tensile stress. A second profile was obtained for each diffusivity after having moved the grid by 1/4 of the spatial period (dashed curves).

whose slope yields the local value of the profile $a_x(x)$, are also reported.

The profiles $a_x(x)$ and $a_z(x)$ were obtained by sliding the Δ-window all the sample along. The profiles in Fig. 13 are those of a particular sample when a 120 MPa tensile stress was applied. In this figure a second couple of profiles can be seen: it was obtained in a second experiment after the mask was moved by a quarter of the grid period. As mentioned before, this second experiment prevented from missing a crack that could be located along one of the symmetry planes of the first heating distribution. Thanks to this double measurement the absence of transverse macro cracks has been verified. By the way, the good repeatability of the analysis could be highlighted.

The evolution of the mean in-plane diffusivity profile with the applied stress is reported in Fig. 14. A progressive decrease of the thermal diffusivity by about 10% can be observed. The decrease is weak and *global, without any marked discontinuity*, until about 10 MPa before failure (this particular sample broke in two parts when stress was set to 130 MPa). This result suggests that *no macro-cracks*

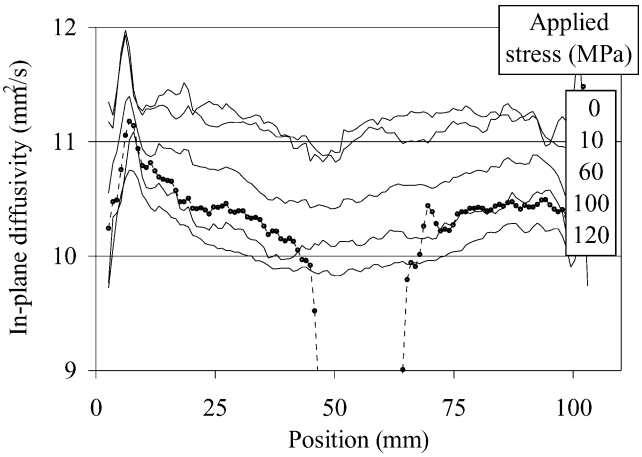

Fig. 14. In-plane thermal diffusivity profiles for different values of the applied stress. The sample broke in two parts for a 130 MPa stress. The profile obtained thereafter is represented with circles.

appeared during most of the stress history and that there was only a progressive *increase of the micro-cracks density*. The through-thickness diffusivity profile also decreased with stress. We noticed a global lowering of this diffusivity, but it reached no more than about 5%. It thus seems that the appearance of transverse micro-cracks is accompanied with the appearance of small in-plane thermal resistances.

After the sample broke, the two parts were joined together and a grid-flash thermography measurement was performed again. With no surprise, the in-plane diffusivity dropped to very low values in a 20 mm wide region centred on the crack position (Fig. 14). Interestingly, outside this region, diffusivity rose back to values higher than those that were observed for a 120 MPa stress. This observation suggests that the stress release induced a partial closure of the micro-cracks.

Similar profiles like those in Fig. 14 were observed for the six other samples. In particular the in-plane diffusivity in the central part of the samples tends to decrease linearly with the applied stress, with an average slope of 0.01 $\mathrm{mm^2{\cdot}s^{-1}}$ per MPa, as illustrated in Fig. 15. There is of course some discrepancy between the seven curves, due to both experimental errors and material properties variations from one sample to the other. Nevertheless, it appears from present measurements that stress can be safely applied until the in-plane diffusivity drops by a little less than 10% from the value corresponding to the as-processed state. If a higher stress is applied, failure is likely to occur soon. The grid-flash thermography technique thus proved to provide an interesting tool for a non-destructive evaluation of the residual life of C/C SiC material.

This technique can be applied with other mask shapes. As a matter of fact, by using a circular mask where the openings are regularly distributed over 360°, one can evaluate simultaneously the through-thickness a_z and the angular diffusivity a_θ of a disk-shaped material. The non-

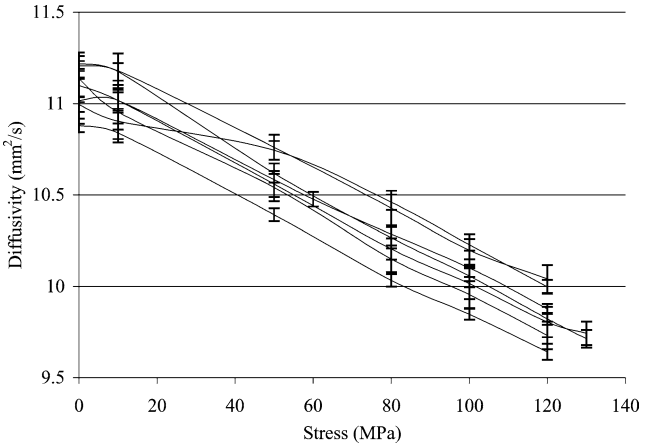

Fig. 15. Mean in-plane thermal diffusivity (between positions 40 and 60 mm) vs. the applied stress for a series of seven C/C-SiC samples up to the stress level just preceding the failure.

destructive full-field characterisation of a carbon brake disk with this approach was described elsewhere [32].

5. Conclusion

We presented the grid-flash thermography technique where a grid-like mask is put between the tested material and the light source (flash lamp or laser beam) while an infrared camera is measuring the temperature distribution evolution on either side of the material (this paper focused on the two-side configuration). The main purpose of this technique is to measure the in-plane diffusivity(ies) in orthotropic material. Incidentally it also allows to measure the through-thickness diffusivity. The in-plane and through-thickness diffusivities can be simultaneously evaluated by analysing a single sequence of thermal images. The principal characteristic is that with the chosen heating distribution every pixel in the image "actively" participates to the in-plane diffusivity identification. We first provided an error analysis for the diffusivity evaluation in homogeneous slabs.

In the case of non-homogeneous materials, the parameter identification can be performed on a local basis in order to yield an approximate diffusivity profile. The local in-plane diffusivity is merely obtained from a linear regression involving the ratio between the local temperature spatial amplitude and the local temperature mean level. The identification procedure was validated on theoretical data that were obtained from numerical simulations. It appears that the inversion gives a smoothed image of the true diffusivity profiles, where smoothing is performed over a width corresponding to one or two grid periods.

Experimental profiles were obtained on C/C-SiC tensile samples during stressing. We essentially noticed a linear and nearly uniform drop of the in-plane diffusivity when stress increased (the diffusivity drop reached about 10% of the initial value when the samples broke). This result is correlated with the fact that, in this particular ceramic matrix composite material, the density of small cracks progressively increases with stress up to failure.

Acknowledgements

Part of this work was performed with financial support of the Deutsche Forschungsgemeinschaft (DFG) in the frame of Sonderforschungsbereich 259 (SFB 259) that the authors gratefully acknowledge. The authors also express their thanks to G. Gardette and F. Passilly for their help during the measurements.

References

[1] C. Hobbs, D.K. Jackson, J. Milne, Quantitative measurement of thermal parameters over large areas using pulse video thermography, in: Proc. of Thermosense XIII Conf., in: SPIE, vol. 1467, SPIE, 1991, pp. 264–277.
[2] S. Ahuja, W.A. Ellingson, J. Stuckley, E.R. Koehl, Determining thermal diffusivity and defect attributes in ceramic matrix composites by infrared imaging, in: Proc. of Thermosense XVIII Conf., in: SPIE, vol. 2766, SPIE, 1996, pp. 249–257.
[3] D. Mourand, J. Gounot, J.-C. Batsale, New sequential method to process noisy temperature response from flash experiment measured by infrared camera, Rev. Sci. Instrum. 69 (3) (1998) 1437–1440.
[4] W.P. Winfree, J.N. Zalameda, Single sided thermal diffusivity imaging in composites with a shuttered thermographic inspection system, in: Proc. of Thermosense XXIV Conf., in: SPIE, vol. 4710, SPIE, 2002, pp. 536–544.
[5] E. Grinzato, S. Marinetti, P.G. Bison, NDE of porosity in CFRP by multiple thermographic techniques, in: Proc. of Thermosense XXIV Conf., in: SPIE, vol. 4710, SPIE, 2002, pp. 588–598.
[6] A. Degiovanni, J.C. Batsale, D. Maillet, Mesure de la diffusivité longitudinale de matériaux anisotropes. Panorama des techniques développées au LEMTA, Rev. Gén. Therm. 35 (1996) 141–147.
[7] E.P. Visser, E.H. Versteegen, J.P. Willem, J.P. Enckevort, Measurement of thermal diffusion in thin films using a modulated laser technique: Application to CVD diamond films, J. Appl. Phys. 71 (1) (1992) 3238–3248.
[8] L. Fabbri, P. Fenici, Three-dimensional photothermal radiometry for the determination of the thermal diffusivity of solids, Rev. Sci. Instrum. 66 (6) (1995) 3593–3600.
[9] D. He, Y. Gu, M. Zheng, D. Zhu, Measurement of thermal diffusivity of thin materials using an infrared thermal wave imaging technique, Progr. Natural Sci. Suppl. 6 (1996) 169–172.
[10] A. Salazar, A. Sanchez-Lavega, A. Ocariz, J. Guitonny, G.C. Pandey, D. Fournier, A.C. Boccara, Thermal diffusivity of anisotropic materials by photothermal methods, J. Appl. Phys. 79 (8) (1996) 3984–3993.
[11] J.-C. Krapez, G. Gardette, Characterization of anisotropic materials by steady-state and modulated thermal ellipsometry, High Temp. High Press. 30 (1998) 567–574.
[12] J.F. Bisson, D. Fournier, Influence of diffraction on low thermal diffusivity measurements with infrared photothermal microscopy, J. Appl. Phys. 83 (2) (1998) 1036–1042.
[13] C.S. Welch, D.M. Heath, W.P. Winfree, Remote measurement of in-plane diffusivity components in plates, J. Appl. Phys. 61 (3) (1987) 895–898.
[14] F. Cernuschi, A. Russo, L. Lorenzoni, A. Figari, In-plane thermal diffusivity evaluation by infrared thermography, Rev. Sci. Instrum. 72 (10) (2001) 3988–3995.
[15] A.B. Donaldson, R.E. Taylor, Thermal diffusivity measurement by a radial heat flow method, J. Appl. Phys. 46 (10) (1975) 4584–4589.

[16] D. Demange, P. Beauchene, M. Bejet, R. Casulleras, Mesure simultanée de la diffusivité thermique selon les deux directions principales d'un matériau, Rev. Gen. Therm. 36 (1997) 755–770.
[17] P. Cielo, L.A. Utracki, M. Lamontagne, Thermal diffusivity measurements by the converging thermal wave technique, Canad. J. Phys. 64 (9) (1986) 1172–1177.
[18] S. Alterowitz, G. Deutscher, M. Gerhenson, Heat capacity and thermal conductivity of sintered Al_2O_3 at low temperatures by the heat pulse technique, J. Appl. Phys. 46 (8) (1975) 3637–3643.
[19] I. Philippi, J.C. Batsale, D. Maillet, A. Degiovanni, Measurement of thermal diffusivities through processing of infrared images, Rev. Sci. Instrum. 66 (1) (1995) 182–191.
[20] R. Osiander, J.W.M. Spicer, J.M. Amos, Thermal inspection of SiC/SiC ceramic matrix composites, in: Proc. of Thermosense XX Conf., in: SPIE, vol. 3361, SPIE, 1998, pp. 339–349.
[21] C. Welch, J. Johnson, Thermographic measurement of in-plane diffusivity in very thin plates using diffusion of thermal patterns, in: D.O. Thompson, D.E. Chimenti (Eds.), Rev. Progress in Quant. Nondestr. Eval., vol. 19, Plenum, New York, 1999, pp. 1449–1456.
[22] J.-C. Batsale, D. Mourand, C. Gobbé, Estimation of thermophysical properties of thin plates with averaging techniques and two temperature model, in: Proc. of QIRT '96, Stuttgart, 1996, in: Eurotherm Series, vol. 50, ETS, Pisa, 1997, pp. 46–51.
[23] Z. Ouyang, F. Zhang, L. Wang, L.D. Favro, R.L. Thomas, Novel measurement of anisotropic thermal diffusivity, in: D.O. Thompson, D.E. Chimenti (Eds.), Rev. Progress in Quant. Nondestr. Eval., vol. 17, Plenum, New York, 1998, pp. 453–456.
[24] W.P. Winfree, D.M. Heath, K.E. Cramer, Thermal diffusivity imaging with a moving line source, in: Proc. of Thermosense XXIII Conf., in: SPIE, vol. 4360, SPIE, 2001, pp. 606–615.
[25] J.-C. Batsale, Real time processing with low cost uncooled plane array IR camera—Some possible linear transformations of data in the case of thermal NDE, Colloquium Lagrangianum, Varenna, 13–15 June 2002.
[26] J.-C. Krapez, Diffusivity measurement by using a grid-like mask, Journée d'Étude de la Soc. Fr. des Thermiciens : Thermographie quantitative, Châtillon, 31 mars 1999.
[27] J.-C. Krapez, Simultaneous measurement of in-plane and out-of-plane diffusivity by using a grid-like mask, in: E. Grinzato, et al. (Eds.), Proceedings of 5th Int. Workshop on Advanced Infrared Techn. and Appl., Venezia, Italy, 1999, pp. 289–296.
[28] J.R. Lesniak, D.J. Bazile, Forced-diffusion thermography technique and projector design, in: Proc. of Thermosense XVIII Conf., in: SPIE, vol. 2766, SPIE, 1996, pp. 210–217.
[29] A. Degiovanni, M. Laurent, Une nouvelle technique d'identification de la diffusivité thermique pour la méthode flash, Rev. Phys. Appl. 21 (1986) 229–237.
[30] J.V. Beck, K.J. Arnold, Parameter Estimation in Engineering and Science, Wiley, New York, 1976.
[31] W. Krenkel, Cost effective processing of CMC composites by melt infiltration (LSI-process), Ceram. Eng. Sci. Proc. 22 (3) (2001) 443–454.
[32] L. Spagnolo, J.-C. Krapez, M. Frieß, H.P. Maier, G. Neuer, Flash thermography with a periodic mask: Profile evaluation of the principal diffusivities for the control of composite materials, in: Proc. of Thermosense XXV Conf., in: SPIE, vol. 5073, SPIE, 2003, pp. 392–400.